Geophysical Prospecting, 1995, 43, 805–829

Elastic anisotropy due to aligned cracks in porous rock[1]

Leon Thomsen[2]

Abstract

All theoretical expressions which relate the characteristics of saturated aligned cracks to the associated elastic anisotropy are restricted in some important way, for example to the case of stiff pore fluids, or of the absence of equant porosity, or of a moderately high frequency band. Because of these restrictions, previous theory is not suitable for application to the upper crust, where the pore fluid is brine ($K_f \approx K_s/20$), the equant porosity is often substantial ($\phi_p > 0.1$), and the frequency band is sonic to seismic. This work removes these particular restrictions, recognizing in the process an important mechanism of dispersion. A notable feature of these more general expressions is their insensitivity, at low frequency, to the aspect ratio of the cracks; only the crack density is critical. An important conclusion of this more general model is that many insights previously achieved, concerning the shear-wave splitting due to vertical aligned saturated cracks, are sustained. However, conclusions on crack orientation or crack aspect ratio, which were derived from P-wave data or from shear-wave 'critical angles', may need to be reconsidered. Further, the non-linear coupling between pores and cracks, due to pressure equalization effects, means that the (linear) Schoenberg–Muir calculus may not be applied to such systems. The theory receives strong support from recent data by Rathore *et al.* on artificial samples with controlled crack geometry.

Introduction

This work concerns the theory of the effect of a set of aligned circular cracks upon the elasticity of the resulting composite material. Of course, the primary effect is a reduction in certain of the elastic moduli, so that the resulting composite material is elastically anisotropic. Assuming that the matrix material is homogeneous and isotropic, the composite material is clearly transversely isotropic, with its symmetry axis lying perpendicular to the flat faces of the cracks. At issue is the dependence of the anisotropy upon angle, upon crack density, upon crack shape, upon stiffness of

[1] Paper presented at the 53rd EAEG meeting, May 1991, Florence, Italy. Received June 1993, revision accepted January 1995.

[2] Amoco Production Company, 4502 East 41st Street, Tulsa, OK, 74102–3385, U.S.A.

the fluid in the cracks, upon the further presence of equant (non-flat) porosity in the rock, and upon frequency.

These topics are reviewed and further developed in the next section. The resulting theory is applied to the propagation of elastic waves, in the asymptotic limit of long wavelengths. The cracks may be conceived as either micro-cracks or 'joints', so long as they are small compared to the seismic wavelength. Only the limiting case of low crack density and thin cracks is considered.

The theory of the effect of cracks on the elasticity of solids has a long history, going back at least to the classic paper by Eshelby (1957). Watt, Davies and O'Connell (1976) gave a theoretical review (in the geophysical context) for isotropic cracks. In all this time, there has been no adequate laboratory confirmation of the theory; this situation has recently been remedied by Rathore *et al.* (1991, 1995). The data, discussed in the last section, strongly supports the theory in its present form.

Small Aligned Crack Density: Arbitrary Porosity

The expressions for the case of small crack density and zero equant porosity are implicit in the work by Walsh (1969) and others of randomly oriented cracks. The case of parallel cracks seems to have been first discussed explicitly, using a scattering formalism, by Garbin and Knopoff (1973, 1975a) for dry cracks and (1975b) for liquid-saturated cracks. Hudson (1980, 1981) developed these ideas further, and they have underlain many contributions by Crampin (e.g. 1981, 1985, 1986) and co-workers.

The effect of equant porosity (i.e. that pore space not characterized as being 'thin and flat' and not having any particular fabric) is not included in this prior work. At first thought, such porosity would not appear to affect the anisotropy, since it does not have any preferred orientation. However, it develops that there is an effect on the anisotropy, caused by fluid flow between cracks and pores; this is a primary subject of the present work.

The subject of weakly anisotropic elastic media with a single axis of symmetry was discussed by Thomsen (1986); the resulting expressions for the phase velocities are

$$\bar{v}_p^2(\theta) = \alpha_0^2[1 + 2\delta \sin^2\theta \cos^2\theta + 2\varepsilon \sin^4\theta] , \tag{1a}$$

$$\bar{v}_{s\perp}^2(\theta) = \beta_0^2\left[1 + 2\frac{\alpha_0^2}{\beta_0^2}(\varepsilon - \delta)\sin^2\theta\cos^2\theta\right] \tag{1b}$$

and

$$\bar{v}_{s\parallel}^2(\theta) = \beta_0^2[1 + 2\gamma \sin^2\theta]. \tag{1c}$$

Here, α_0 and β_0 are the P- and S-wave velocities in the symmetry direction; θ is the angle between the wavefront normal and the symmetry axis. The shear mode S$\parallel$ is

polarized parallel to the symmetry planes (i.e. to the cracks); the shear mode S⊥ is polarized orthogonal to S∥, with a non-zero component perpendicular to the symmetry plane. (These are sometimes called SH and SV, respectively, but this notation is confusing when, as in this case the symmetry plane is not necessarily horizontal.) Here, the anisotropy parameters α, β and γ are assumed to be small ($\ll 1$) and mutually independent.

In the case where the anisotropy is caused by aligned cracks, the anisotropy parameters may be further specified. Assuming that the cracks are circular ellipsoids ('penny-shaped'), perfectly aligned and sparsely distributed in a porous medium composed of isotropic grains, it is shown in the Appendix § II that the anisotropies are given by

$$\varepsilon = \left(\frac{8}{3}\right)\left(1 - \frac{K_f}{K_s}\right) D_{cl}\left[\frac{(1 - \nu^{*2})E}{(1 - \nu^2)E^*}\right]\eta_c, \tag{2a}$$

$$\gamma = \left(\frac{8}{3}\right)\left(\frac{1 - \nu^*}{2 - \nu^*}\right)\eta_c, \tag{2b}$$

and

$$\delta = 2(1 - \nu)\varepsilon - 2\left(\frac{1 - 2\nu}{1 - \nu}\right)\gamma. \tag{2c}$$

In (2), K_s is the incompressibility of the solid grains, K_f is that of the fluid in the cracks, ν is the Poison's ratio of the isotropic porous rock (without the cracks), E is its Young's modulus, ν^* and E^* are the corresponding properties of the dry isotropic porous rock.

Under these assumptions, the anisotropies (2) are each linear in the fracture density η_c, which may be written in terms of the number density of cracks N_v and their mean cubed diameter as

$$\eta_c = N_v\left\langle\frac{a^3}{8}\right\rangle, \tag{3a}$$

or equivalently in terms of the crack porosity ϕ_c and aspect ratio c/a thickness/diameter) of the cracks as

$$\eta_c = \frac{3}{4\pi}\frac{\phi_c}{(c/a)}. \tag{3b}$$

The properties of the isotropic porous rock (without the cracks) may be derived from the measured rock properties (cf. Appendix § I) using

$$\beta = \sqrt{\frac{\mu}{\rho}} = \bar{v}_{s\parallel}(90°) \tag{4a}$$

and

$$\alpha = \sqrt{\frac{\left(K + \frac{4\mu}{3}\right)}{\rho}} = \bar{v}_p(90°)\left[\frac{1 + 2\varepsilon(1-v)^2/(1-2v)}{1+2\varepsilon}\right]^{1/2}$$
$$\approx \bar{v}_p(90°)\left[1 + \frac{v^2}{1-2v}\,\varepsilon\right], \tag{4b}$$

where μ is the shear modulus and v and E may be found in the usual isotropic way. Evidently (cf. (2a)), the Poisson's ratio v of the isotropic porous rock appears in a way which requires a short iteration loop for the calculation of α; for small crack density, this is not a serious problem. The properties of the dry isotropic porous rock (if not measured) may be estimated in a conventional way, e.g. using the method of Biot (1941) and Gassmann (1951) or Mavko and Jizba (1991); the imprecision thus incurred is not significant to the anisotropic conclusions.

The principal contribution of this work consists in the derivation (Appendix § II) of the 'fluid influence factor' D_{ci} of (2), specified (in the limit of low frequency) by

$$D_{ci}(\text{lo}) = \left[1 - \frac{K_f}{K_s} + \frac{K_f}{K^*\phi}\left\{\left(1 - \frac{K^*}{K_s}\right) + A_c(v^*)\eta_c\right\}\right]^{-1}, \tag{5a}$$

where K^* is the incompressibility of the dry isotopic porous rock and ϕ is the total porosity (cracks plus pores, etc.) of the rock. A_c is a known function of v^*, given by (A26b). The subscript on D_{ci} indicates that it refers to cracks in an isotropic medium of arbitrary isotopic porosity, perhaps including equant pores, randomly orientated cracks and pore throats, all hydraulically connected. (In particular, there is no limitation to finite ϕ, as all the effects of finite porosity are contained within the phenomenological parameter K^*.)

In this context, 'low frequency' means low enough for the fluid pressure to have time to equilibrate locally between cracks and adjacent pores. That is, it is much less than the 'squirt frequency', a characteristic rock property which depends on the details of the crack-pore microgeometry and the properties of the fluid. The squirt frequency can be estimated by various model theories (see e.g. O'Connell and Budiansky 1977; Mavko and Jizba 1991) and usually lies somewhere between the sonic and ultrasonic bands, for brine-filled rocks. Hence, for application to seismic band data, the low-frequency approximation is appropriate. Further constraints on the squirt frequency are outside the scope of the present paper.

At 'moderately high' frequencies, where the fluid does not have time to flow at all between various portions of the local microgeometry, the expression of D_{ci} is (see Appendix II) given by

$$D_{ci}(\text{mh}) = \left[1 - \frac{K_f}{K_s} + \frac{K_f}{K^*}\left\{A_c(v^*)\,\frac{\eta_c}{\phi_c}\,\frac{(1 - K_f/K_s)}{(1 - K_f/K)}\right\}\right]^{-1}. \tag{5b}$$

The 'moderately high' frequency approximation is useful in analysing ultrasonic data. At still higher frequencies (O'Connell and Budiansky 1977), the shear stress in the fluid is unrelaxed (due to the fluid viscosity) and at the highest frequencies, Rayleigh scattering becomes important. These high frequencies are excluded from the present analysis.

The principal difference between (5a) and (5b) is that the porosity (which appears in the denominator within the square brackets) is the total porosity ϕ in the low-frequency case (5a), and the crack porosity ϕ_c in the 'moderately high' frequency case (5b). Since these two porosities usually differ greatly, the numerical consequences of this difference are substantial. Physically, these two porosities identify the volumes of fluid which are pressurized by deformation of the cracks (during wave propagation): the entire pore volume in the low-frequency case, and the cracks alone in the 'moderately high' frequency case.

In order to understand the meaning of these equations, it is useful to consider some special cases. First, consider the case where the equant porosity is small ($<10\%$), so that its effects may be modelled, just as the aligned cracks are modelled. In this case (see Appendix § III), the anisotropies may be written

$$\varepsilon = \frac{8}{3}\left(1 - \frac{K_f}{K_s}\right) D_{cp}\,\eta_c\,, \tag{6a}$$

$$\gamma = \frac{8}{3}\left(\frac{1 - \nu_s}{2 - \nu_s}\right)\eta_c\,, \tag{6b}$$

$$\delta = 2(1 - \nu_s)\varepsilon - 2\left(\frac{1 - 2\nu_s}{1 - \nu_s}\right)\gamma, \tag{6c}$$

where η_s is the Poisson's ratio of the solid. The fluid influence factor D_{cp}, whose subscript indicates that both cracks and pores are modelled, is given by

$$D_{cp}(\text{lo}) = \left[1 - \frac{K_f}{K_s} + \frac{K_f}{K_s(\phi_p + \phi_c)}\left\{A_p(\nu_s)\phi_p + A_c(\nu_s)\eta_c\right\}\right]^{-1}, \tag{7a}$$

$$D_{cp}(\text{mh}) = \left[1 - \frac{K_f}{K_s} + \frac{K_f}{K_s\phi_c}\left\{A_c(\nu_s)\eta_c\right\}\right]^{-1} = D_c\,, \tag{7b}$$

where A_p is a corresponding coefficient (defined in (A30b)), and ϕ_p is the isotropic equant porosity, modelled as isolated spheres.

Next, consider the limiting case of zero equant porosity, obtained from (7) by setting $\phi_p = 0$. In this case (with fluid influence factor D_c), the two formulae coincide, as given by (7b); there is no dispersion due to fluid-flow effects across this frequency range. This approximation, with zero ϕ_p, is similar to that of Hudson (1981, §3.3, as specialized to a liquid, i.e. with negligible shear modulus of the crack-filling material).

Hudson (1981) restricted his derivation to long wavelengths, i.e. to $ka/2 \ll 1$, where k is the shear wavenumber. Hence, his treatment is often characterized as a 'low-frequency' approximation. However, it is clear from the present discussion

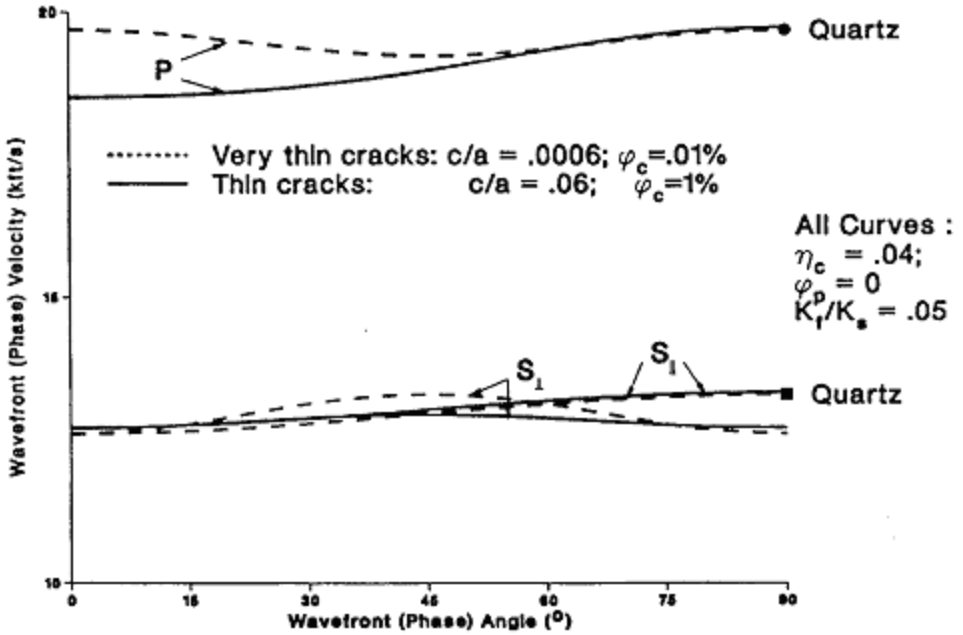

Figure 1. Effect of aspect ratio on crack-induced anisotropy. Linearized theory: quartzite/brine example.

that, when applied to materials with a complex pore-space (e.g. rocks), it is valid only for frequencies which (while still meeting the criterion above) are higher than the squirt frequency, so that the pore-space does not affect the fluid pressure in the cracks. In this context, it is more properly called a 'moderately high-frequency' approximation.

Note the appearance in (7b) of the factor

$$\frac{K_f \eta_c}{K_s \phi_c} = \frac{3}{4\pi} \frac{K_f}{K_s} \frac{1}{c/a}, \tag{8}$$

first recognized (and denoted $3\omega/4\pi$) by O'Connell and Budiansky (1974). This combination of parameters controls the shape of the $\bar{v}_p(\phi)$ curve strongly, and the $\bar{v}_s(\phi)$ curve to a lesser degree, in this case.

In the limit of very thin cracks, i.e. those with very small aspect ratio,

$$\frac{c}{a} \ll \frac{4}{3\pi} \frac{K_f}{K_s} \left(\frac{1 - v_s^2}{1 - 2v_s} \right) \approx \frac{1}{30}, \tag{9}$$

the fluid influence factor D_c (see (7b)) vanishes, meaning that the anisotropy parameter ε vanishes also (cf. (6a)). With constant crack density η_c, this is also the limit of infinitesimal crack porosity ϕ_c, and of stiff fluid incompressibility, $K_f = K_s$.

The approximation, with vanishing D_c, is similar to that of Hudson (1981, §3.1). Note the approximation (9) is a much stronger condition than may be casually

understood by the term 'thin cracks' (i.e. $c/a \ll 1$). Nonetheless, Crampin and co-workers (especially pre-1984) achieved great insights via application of this (Hudson) approximation in the interpretation of shear-wave splitting.

However, the vanishing ε (which means that P-waves travelling across the cracks are not slower than those travelling along the cracks) is counter-intuitive. More importantly, actual field data (e.g. Shear and Orcutt 1985, 1986; Stephen 1985; White and Whitmarsh 1984) often show $\varepsilon \neq 0$, in contexts where empty or gas-filled cracks are not plausible, so that this limiting case is not appropriate.

Crampin *et al.* (1986) noted that Hudson's (1981, §3.3) equations permit non-zero ε if the aspect ratio c/a is sufficiently large, i.e. (in the present context) if approximation (9) is not met. However, if equant porosity is present, (6) and (7a) show that at low frequencies, the effect of cracks is to require $\varepsilon \neq 0$ always, independent of aspect ratio, even when the fluid is brine. This point is illustrated here by two specific calculations which illustrate the effect of equant porosity.

Figure 1 shows the theoretical low-frequency phase velocities calculated with (1), (6), (7), using the parameters of a typical crystalline rock ($\phi_p = 0$), saturated with brine. The figure shows two cases with different ϕ_c (or equivalently, different c/a) at fixed η_c. The angular dependence of $\bar{v}_p$ is qualitatively dependent upon c/a, and that of $\bar{v}_{s\perp}$ (hence of the critical angle where the two shear velocities are equal,) is quantitatively dependent. Crampin (1984, 1986) utilized Hudson's (1981) corresponding equations (including this degree of freedom) to model field data, thereby deducing a value of *in situ* crack aspect ratio.

However, Fig. 2 shows the same calculations, with the same material parameters, except with 10% equant porosity. The figure illustrates the insensitivity of these calculations to aspect ratio; the dashed curves (for very thin cracks) are negligibly different from the solid curves (for nominally thin cracks). Numerically, this happens because the porosity in the denominator of (7a) is total (modelled) porosity $\phi_p + \phi_c$, not crack porosity ϕ_c. Hence, this result, and the following discussion, apply equally as well to the more general case, equations (1), (2), (4) and (5a) with arbitrary equant porosity. A similar effect is seen if the fluid in the pore space has a very low incompressibility K_f, e.g. if it is a gas.

The non-trivial effect on anisotropy of the equant porosity, although counter-intuitive at first, may be understood physically as follows. An empty crack is compliant because of its 2D shape; equant pores are stiffer. If the crack is isolated, or connected only to other cracks of similar shape and orientation, then a saturating liquid can significantly stiffen the crack, because of the incompressibility K_f of the liquid. However, if the crack is connected to the equant pore space, then as a P-wave passes, the liquid will 'squirt' into the pore space (which is less compilant than the crack) instead of stiffening the crack. Hence, because of this fluid pressure equilization, the pores do affect the compilance of the cracks, and hence the anisotropy.

Therefore, it follows that the special case of crack-induced anisotropy with small or zero values for the anisotropy parameter ε is not appropriate for most upper

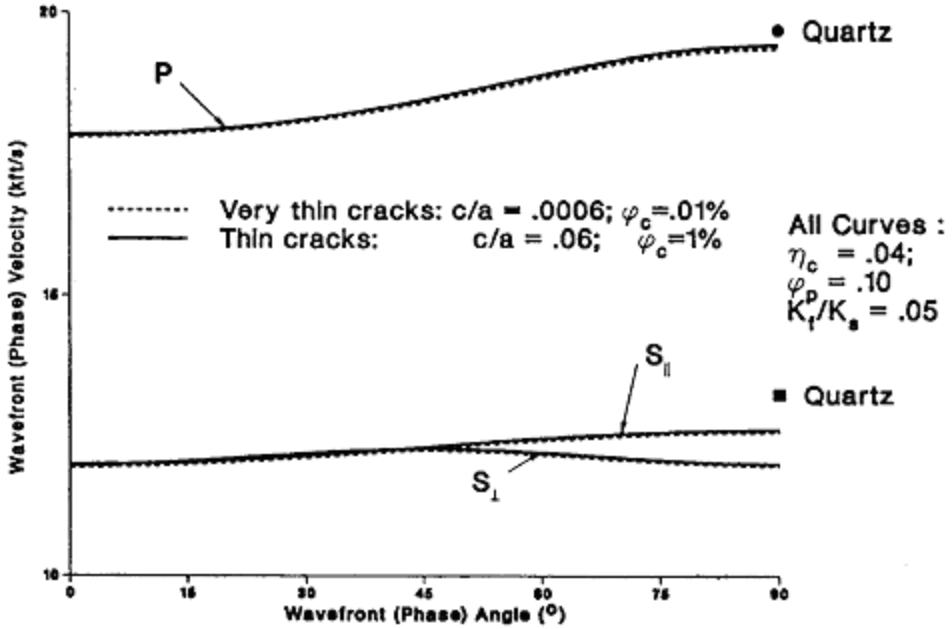

Figure 2. Small effect of aspect ratio when equant porosity is present. Linearized theory: sandstone/brine example.

crustal contexts where equant porosity is non-negligible, and the pore-filling fluid is brine or oil. This applies especially where P-waves are a primary data set. Because of trigonometric identities, this implies that there should be a substantial 2θ variation (comparable to the 4θ variation) in such P-wave velocities, due to a single set of vertical saturated cracks.

It is also clear from Fig. 2 that the critical angle (where the two shear modes have equal velocities) is not a strong function of the crack aspect ratio. Therefore, this critical angle may not be reliably used to estimate the aspect ratio.

The fluid pressure equalization discussion here will also occur if cracks of differing shape (and hence, differing compliance) are present and hydraulically connected. In fact, it is easy to generalize these results to the case of a distribution of crack shapes c/a, all aligned in the same direction (just replace η_c everywhere by an appropriate integral over the distribution).

Further, if multiple crack-sets exist, with differing orientations, a similar consideration is required. That is, not only will the symmetry be lower, in general than that considered here, but also fluid pressure equalization in the intersecting cracks will affect each of the corresponding fluid influence factors. Thus, the treatment of Crampin (1978), ignoring this effect, is appropriate only for unsaturated cracks or hydraulically unconnected cracks. A correct treatment, although outside the scope of this paper, may be found as a straightforward extension of these ideas.

It further follows, because of this non-linearity in the crack-pore-crack fluid interaction, that the linear calculus of Schoenberg and Muir (1989) is not applic-

able in this context. That is, the compilance of one structural element (e.g. pores or cracks) depends upon the existence and compliance of other elements (if they are saturated and hydraulically connected) so that they may not be linearly superposed. It is well known that further non-linearities arise from finite values of ϕ_i and η_c, whether or not they are saturated or hydraulically connected (cf. e.g. O'Connell and Budiansky 1974).

Data and Discussion

This work continues a line of thought established by the classic paper of Eshelby (1957). Over the years, there has been a vigorous theoretical discussion, particularly focused on isotropic cracks and on the issue of substantial crack density (not addressed here). But in all this time, there has been no strong laboratory confirmation of rejection of the (original or subsequent) theoretical claims. The difficulty has been in the determination of the microscopic structure of the cracks: their shape, size, orientation and distribution. Without such prior determination, the parameters of the theory are free for fitting, thus reducing the predictive power of the theory.

This situation was changed by Rathore *et al.* (1991, 1995), who developed techniques for manufacturing artificial samples with known crack geometries. Previously (for example), artificial aligned 'cracks' had been constructed by stacking together pieces of glass, with the shape of the cracks determined by the unknown topography on the glass surfaces. By contrast, the technique of Rathore *et al.* (1991, 1994) was to construct an artificial porous rock by glueing together grains of sand, with imbedded discs of metal of known size, shape, orientation and distribution. These metal discs were then leached out chemically, leaving disc-shaped voids, with the sandstone porosity and permeability providing leachant access to the discs.

Representative data from Rathore *et al.* is shown below (both saturated and dry, in both frequency ranges), at various angles of propagation, with comparisons to the present theory, equations (1)–(5), and to the theory of Hudson (1981, §3.3). In the comparisons, the theory is fitted to the data in the crack-parallel direction; the anisotropic variation is then an unfitted prediction of each theory. The parameters thus fitted are indicated graphically in the figures (near 90°), and are listed in Table 1.

For the Hudson theory, the anisotropy parameters shown in Table 1 are defined similarly to those of equation (1), but are normalized by the crack-parallel velocities, instead of the crack-normal velocities, following Hudson. Also, in fitting the Hudson theory, the 'Solid_H' properties are fitted independently in the dry and saturated cases, regarding in each case the porous framework as the 'solid' of the theory. For the present theory, the two fits are related by the Biot-Gassmann theory. The well-known shortcomings, at finite frequencies, of the Biot-Gassman theory (cf. e.g. Thomsen 1985) are reflected in an apparent frequency-dependence

Table 1. Parameters: input and derived

Input rock parameters			Input crack parameters	
	Dry	Saturated		
V_p (90°) (km/s)	2.56	2.67	crack density η_c	0.100
$V_{s\|\|}$ (90°) (km/s)	1.52	1.41	crack porosity ϕ_c	0.0023
K_f (Mpsi)	0.0	0.32	aspect ratio c/a	0.0036
ρ (g/cm^3)	1.722	2.072	equant porosity ϕ_p	0.35

	Thomsen: Equations (1)–(5)		
	Saturated, low frequency (Fig. 3a)	Saturated, moderately high frequency (Fig. 3b)	Dry (Figs 5a, b)
α_0 (km/s)	2.38	2.07	2.07
β_0 (km/s)	1.27	1.37	1.37
ε	0.139	0.005	0.267
δ	0.091	−0.097	0.277
γ	0.115	0.115	0.115
ν	0.321	0.307	0.241
α (km/s)	2.75	2.67	2.61
β (km/s)	1.41	1.41	1.52
K_s (Mpsi)	4.55	3.19	—

	Hudson (1981, §3.3)	
	Saturated (Figs 3a, b)	Dry (Figs 5a, b)
α_0 (km/s)	2.67	2.65
β_s (km/s)	1.41	1.52
ε_H	0.006	0.267
δ_H	−0.113	0.248
γ_H	0.109	0.114
ν_s (f)	0.307	0.254

of the inferred K_s (cf. Table 1); this is viewed as being numerically insignificant to the present argument.

Figure 3a shows the saturated case, with the 'data' representing the first breaks of the waveforms taken to correspond to the arrivals of the highest frequencies with significant power (about 80 kHz). The figure also shows calculations (as above) from both theories, which agree closely with each other in this case, and with the data.

It deserves emphasis that neither the P-wave nor shear-wave anisotropic variation (including the shear-wave splitting) was fitted here in any way. With the

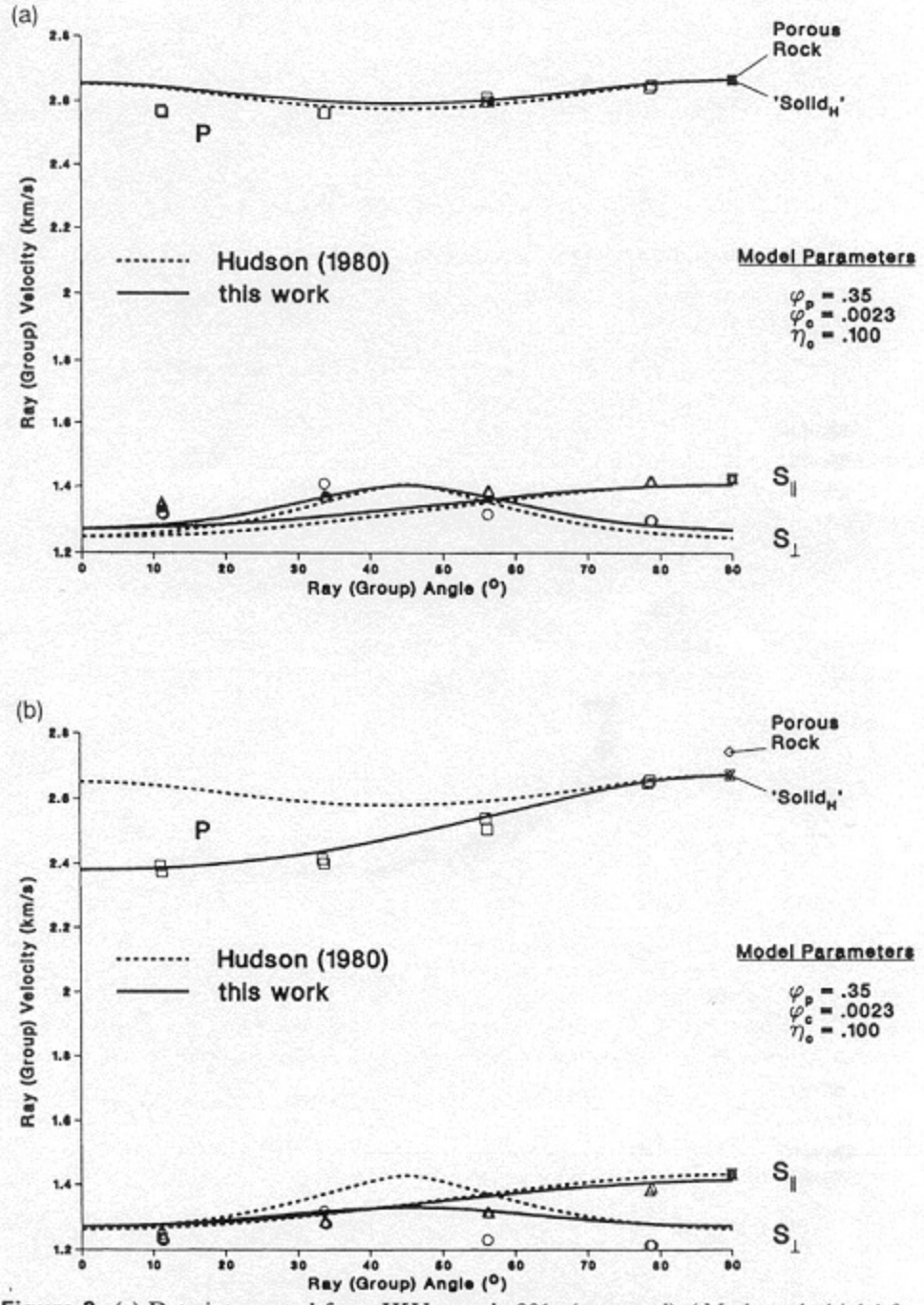

Figure 3. (a) Data interpreted from IKU sample 901c (saturated). 'Moderately high' frequency. (b) Data interpreted from IKU sample 901c (saturated). 'Low' frequency.

known crack (and pore) geometry, there were no free model parameters for fitting the anisotropy.

Figure 3b shows the saturated 'data' at low frequencies; this is the case of greatest interest for interpreting seismic data. As expected from the previous theoretical discussion, the principal effect of the fluid pressure equilibration at low frequencies is on the P-wave anisotropy and on the critical angle (where the two shear waves have equal velocities). It is clear from the waveforms (see below) that there is significant angle-dependent attenuation and dispersion. The theory of Hudson (1981) includes attenuation due to scattering (the high-frequency effect mentioned above), but explicitly neglects the corresponding dispersion; the dashed curves are the same as in Fig. 3a. The present theory does recognize dispersion in this frequency range; Fig. 3a uses (7b), whereas Fig. 3b uses (7a). The 'data' show good agreement with the present theory (solid curves), in its low-frequency form.

The 'data' in Fig. 3b are interpreted from the same waveforms as the 'data' of Fig. 3a; they are representative of the lowest frequencies present (about (30 kHz). These are interpreted from the wave-forms in a conventional way, by subtracting from the high-frequency velocity a dispersion term calculated from the measured attenuation. In general, the interpreted velocity at a given low frequency f_0 depends upon the dispersion, hence the attenuation, at all frequencies between f_0 and the high frequency f_1 of the measurement. Since attenuation information is only available in the frequency band of the data, it is not possible to correct to zero frequency, but only to the lowest frequencies f_0 of the data. For each angle of propagation, one may estimate the dispersion by

$$v(f_0) = v(f_1)\left(1 + \frac{1}{\pi \bar{Q}} \ln\left(\frac{f_0}{f_1}\right)\right) \tag{10}$$

(see Aki and Richards 1980, §5.5.2), where f_0 is the low frequency identified above, f_1 is the high frequency, and $\bar{Q}$ is the average quality factor in the interval (f_0, f_1). This formula is formally limited to large $\bar{Q}$ and to isotropic materials. Nevertheless, it is used here, independently for each angle of propagation, to estimate the low-frequency velocities. The resulting corrected data are those shown and compared with theory in Fig. 3b. Rathore *et al.* (1991, 1995) pick the low-frequency arrivals directly from the waveform data; the results are qualitatively consistent with the present technique (high-frequency picks, dispersion correction).

Because the dispersion corrections are so substantial, Fig. 4 shows the transmitted P-wave forms (for each angle of propagation), with deduced values of $\bar{Q}$ for each. These attenuation data represent the average Q over the bandwidth of significant energy, i.e. 30–80 kHz for this data. It is obvious, from visual inspection, that the arrival of the bulk of the energy (for the waves travelling across the cracks) is delayed, even though the first breaks are not. The procedure indicated above, equation (10), merely quantifies this; the results are recorded in Fig. 3b.

It deserves emphasis that the data correction here was not adjusted to match the data, but comes independently from the estimates of Q (Fig. 4), and the bandwidth

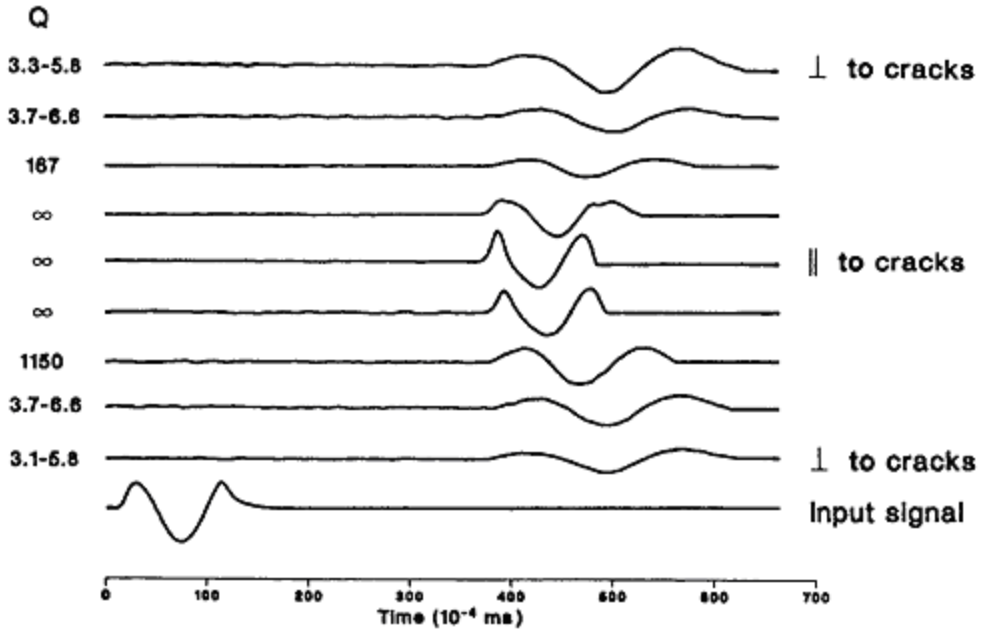

Figure 4. IKU sample 901c, saturated: P waveforms versus angle of incidence to crack-planes.

of the data. The apparent high accuracy of prediction by the present theory is probably fortuitous, as the procedure described here probably represents a minimal correction. Nevertheless, the sign and approximate magnitude of the required correction are surely correct.

Turning now to the dry case, Fig. 5a shows 'moderately high' frequency data (first breaks), together with the two theoretical calculations. In this case, the anisotropy is large ($\varepsilon = 23\%$), so the neglect of non-linear terms (by both theories) is not really justified, and only qualitative agreement with the data should be expected. Nonetheless, the present theory does show good quantitative agreement, in both the P-wave and the shear-wave anisotropy. Hudson's theory severely overestimates the P-wave anisotropy, but accounts for the shear-wave anisotropy well.

Figure 5b tells a similar story, but here the 'data' are representative of the lowest frequencies in the data. The low-frequency velocities were calculated from the data in Fig. 5a and the observed attenuation, as above; since the corrections are minor, the corresponding waveforms are not shown. Neither theory contains any provision for dispersion in dry rock, hence the theoretical curves are the same as in Fig. 5a. Since the velocity corrections are minor, the agreement with theory remains surprisingly good.

These data (particularly the saturated data) are interpreted as offering strong support for the theory, in its present form. In fact, these data, based on artificial

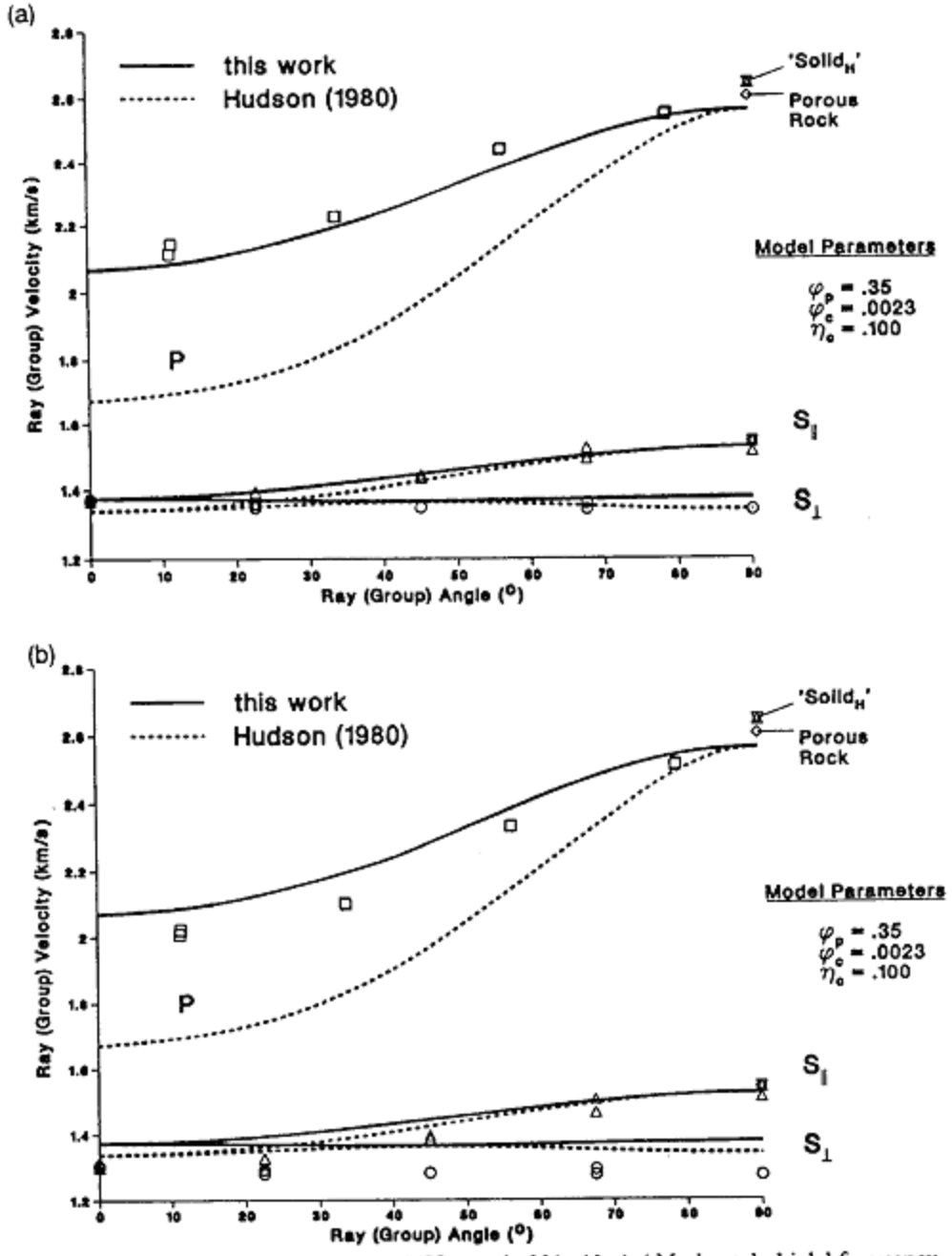

Figure 5. (a) Data interpreted from IKU sample 901c (dry). 'Moderately high' frequency. (b) Data interpreted from IKU sample 901c (dry). 'Low' frequency.

rocks with controlled crack geometry, represent the first strong confirmation of the theory of Eshelby (1957) and the many subsequent theorists who built upon this classic paper. The confirmation is 'strong' because no free model parameters are available to fit the data, yet the predictions are quantitatively accurate.

Of course, real rocks do not have idealized crack-shapes as did the artificial rocks of Rathore *et al.* However, this experimental verification of the theory lends confidence to its estimation of 'effective' crack parameters in the real rocks. For example, the theory says that the details of the crack shape are unimportant, so long as the cracks are thin (with equant porosity present, not even their aspect ratio is important). It is clear that the techniques of Rathore *et al.* may be used to test this proposition further; if verified, it means that the complicated shapes of natural cracks may be effectively modelled by the simple theory.

For application to most crustal rocks (with non-negligible equant porosity), the present generalization of Eshelby's (1957) work is important, as it helps avoid misinterpretation of field data. Since each of the various anisotropy parameters (2) is linear in crack density η_c, their relative sizes depend only on the Poisson's ratio of the uncracked rock, and the other parameters contained in the fluid influence factor D_{ei} (5a). The correct form of D_{ei} avoids the possibility of erroneously concluding, for example, that a large relative magnitude of ε or δ implies gas in the cracks (White and Whitmarsh 1984).

The present work is also important (in most crustal applications) in the physical interpretation of the critical angle (where the two shear modes have equal velocities), and in the analysis of multiple crack-sets, following the discussion in the previous section.

Finally, it highlights the role of the pore fluid, and shows how fluid 'squirt' between various portions of the pore-space (a well-known effect in isotropic rocks, and a dominant mechanism of attenuation) also affects the anisotropy, in a frequency-dependent way.

Acknowledgements

S. Cardimona (UT), S. Crampin (BGS), E. Fjaer (IKU), G. Mavko (Stanford), R. O'Connell (Harvard), J. S. Rathore (Amoco), and M. Schoenberg (SDR) have provided useful discussions of these concepts. I thank I. Tsvankin (now at CSM) for the dispersion corrections. The essence of this theory was presented at the 2nd international workshop on seismic anisotropy, Moscow, 1986, at the AGU fall meeting, San Francisco, 1986, and at the EAEG meeting, Florence, 1991.

Appendix

Derivations

I. Solid matrix

This derivation specializes, generalizes, clarifies and corrects the work of Hoenig

(1978, 1979); we consider first the case of cracks only. The elastic compliance tensor M_{ijkl} of a transversely isotropic body may be written as a two-dimensional symmetric matrix $M_{\alpha\beta}$ following the usual Voigt recipe:

$$\mathbf{M} = \begin{bmatrix} \frac{1}{E_{11}} & \left(\frac{1}{E_{11}} - \frac{1}{2\mu_{66}}\right) & -\frac{1}{E_{13}} & & & \\ & \frac{1}{E_{11}} & -\frac{1}{E_{13}} & & & \\ & & \frac{1}{E_{33}} & & & \\ & & & \frac{1}{\mu_{44}} & & \\ & & & & \frac{1}{\mu_{44}} & \\ & & & & & \frac{1}{\mu_{66}} \end{bmatrix}. \tag{A1a}$$

Only the non-zero elements of the upper triangle are shown. There are five independent elastic compliances.

If the anisotropy is caused by parallel cracks lying in the 3-plane of an isotropic solid, then the only strain components affected by the cracks have subscripts 13, 23 and 33 (the last only when the stress is also 33). In this case, (A1a) reduces to the special form

$$\bar{\mathbf{M}} = \begin{bmatrix} 1/E_s & -\nu_s/E_s & -\nu_s/E_s & & & \\ & 1/E_s & -\nu_s/E_s & & & \\ & & 1/\bar{E} & & & \\ & & & 1/\bar{\mu} & & \\ & & & & 1/\bar{\mu} & \\ & & & & & 1/\mu_s \end{bmatrix}, \tag{A1b}$$

which has only four independent elastic compliances, two of which are shown as the elastic moduli E_s and μ_s of the uncracked solid. Its Poisson's ratio ν_s has the usual connections with the isotropic solid moduli:

$$\nu_s \equiv \frac{E_s}{2\mu_s} - 1 = \frac{1}{2} - \frac{E_s}{6K_s}. \tag{A2}$$

The reduction in degrees of the freedom (from 5 to 4) represented by (A1b) results in a constraint among the five elastic moduli, independent of any particular model for the cracks, so long as they are thin and parallel. This constraint may be written

in terms of the elastic moduli as

$$C_{33}C_{11} - C_{13}^2 = 2C_{66}(C_{33} + C_{13}). \tag{A3}$$

The cracks affect only the two quantities $\bar{E}$ and $\bar{\mu}$. Before deriving velocities, we discuss and refine Hoenig's (1978, 1979) results for these crack-weakened moduli.

Using only elementary operations of volumetric averaging (following arguments established by Hill 1963), Hoenig (1979) derived (his equation (2.14')) an expression equivalent to

$$\bar{M}_{ijmn}\bar{\sigma}_{mn} = M^s_{ijmn}\bar{\sigma}_{mn} + \phi_c\langle\varepsilon^c_{ij}\rangle + \phi_c p_f M^s_{ijkk}, \tag{A4}$$

where the brackets indicate a volumetric average and repeated subscripts imply summation. The symbol ε^c_{ij} refers to a component of the strain in the cracks, resulting from the far-field application of the average stress $\bar{\sigma}$. p_f is the corresponding fluid pressure increment in the cracks; it is uniform if, as assumed at this stage, the cracks are all of the same shape.

From (A4), one may form special cases corresponding to simple stresses. For a pure shear (13) stress,

$$\bar{\sigma}_{mn}(13) = \bar{\sigma}_{13}(\delta_{m1}\delta_{n3} + \delta_{m3}\delta_{n1}).$$

(The explicit argument 13 simply indicates which special case is considered.) The corresponding compliance is

$$\frac{1}{\bar{\mu}} = \bar{M}_{44} = \bar{M}_{1313} = \frac{1}{\mu_s} + \left\langle \frac{\varepsilon^c_{13}(13)}{2\bar{\sigma}_{13}} \right\rangle \phi_c. \tag{A5}$$

Because of the form of (A4), it is easier to write the equation for $\bar{E}$ first in terms of the anisotropic bulk modulus, i.e.

$$\frac{1}{\bar{K}} \equiv \bar{M}_{jjmm} = \frac{2}{E_s} + \frac{1}{\bar{E}} - \frac{6\nu_s}{E_s} = \frac{1}{K_s} + \frac{1}{\bar{E}} - \frac{1}{E_s}, \tag{A6}$$

where the last form uses (A2). For a pure compressive stress, $\bar{\sigma}_{mn}(jj) = -\bar{p}\delta_{mn}$, summing (A4) yields

$$\frac{1}{\bar{K}} = \frac{1}{K_s} + \phi_c\left\langle \frac{\varepsilon^c_{mm}(jj)}{-\bar{p}} \right\rangle - \frac{p_f\phi_c}{\bar{p}K_s}. \tag{A7}$$

Addressing the issue of saturation with a fluid of non-negligible K_f (e.g. brine), we consider first the bulk modulus. The effects of fluid in a poroelastic medium were given by Biot (1941) and Gassmann (1951), who assumed a uniform p_f. Their results may be used here (despite the lack of hydraulic connectivity in this case with isolated cracks), because all the cracks have the same shape (thus assuring that p_f is uniform). (The next section treats a more realistic model.) The (Biot–Gassmann) fluid pressure may be written in terms of the pore strain (cf. Thomsen

1985 as

$$\frac{p_f}{\bar{p}} = \left[\frac{1}{\bar{K}^*} - \frac{1}{K_s} - \phi\left\langle\frac{\varepsilon^p_{mm}(jj)}{-\bar{p}}\right\rangle\right] \Big/ \left[\frac{1}{\bar{K}^*} - \frac{1}{K_s} - \frac{\phi}{K_s}\right]. \tag{A8}$$

Here, the strain with superscript^p refers to the entire pore space (isotropic or not) and ϕ is the total porosity; this generality will be useful later. The asterisk indicates a property of the dry state ($K_f = 0$). In the undrained case, $p_f = -K_f\langle\varepsilon^p_{mm}(jj)\rangle$ and (A8) leads to

$$\phi\left\langle\frac{\varepsilon^p_{mm}(jj)}{-\bar{p}}\right\rangle - \frac{p_f\phi}{\bar{p}K_s} = \left[\frac{1}{\bar{K}^*} - \frac{1}{K_s}\right]\left(1 - \frac{K_f}{K_s}\right)D_p, \tag{A9a}$$

where

$$D_p = \left[1 - \frac{K_f}{K_s} + \frac{K_f}{\phi}\left(\frac{1}{\bar{K}^*} - \frac{1}{K_s}\right)\right]^{-1}. \tag{A9b}$$

In the present context, all the porosity is contained within the cracks. Hence, using (A9) in (A7), we have

$$\frac{1}{\bar{K}} = \frac{1}{K_s} + \left(1 - \frac{K_f}{K_s}\right)\phi_c\left\langle\frac{\varepsilon^c_{mm}(jj)}{-\bar{p}}\right\rangle^* D_p. \tag{A10}$$

For the undrained saturated shear modulus, a derivation along the lines of (A8)–(A10) may be performed by inspection. Replacing the compressional stress, strain and moduli with shear equivalents, and recognizing that $\mu_f/\mu_s = 0$, one sees immediately that the shear equivalent of D_p is unity and hence that $\bar{\mu} = \bar{\mu}^*$.

The problem is thus reduced, without further approximation, to finding the stress-strain ratios in the dry cracks (in brackets above, (A5) and (A10)). These are found by solving the associated 'canonical problem' of a single crack in an otherwise uniform isotropic body subjected to constant far-field stress. For empty circular ellipsoidal (penny-shaped) cracks, Hoenig (1978, 1979) finds (with a slight notation change) that

$$\left\langle\frac{\varepsilon^c_{13}(13)}{2\bar{\sigma}_{13}}\right\rangle^* = \frac{1}{4(c/a)E_s}\bar{\beta}^*_2 \tag{A11a}$$

and

$$\left\langle\frac{\varepsilon^c_{mm}(jj)}{-\bar{p}}\right\rangle^* = \left\langle\frac{\varepsilon^c_{33}(33)}{-\bar{p}}\right\rangle^* = \frac{1}{(c/a)E_s}\bar{\beta}^*_3, \tag{A11b}$$

where c/a is the crack aspect ratio. The dimensionless 'crack displacement magnitudes' $\bar{\beta}^*_j$ are given by Hoenig (1978) in the self-consistent approximation, i.e with finite crack density η_c (cf. (3)). (Note, however, that Hoenig (1978) implicitly retained the modulus E_s in (A11), even at large η_c, instead of replacing it with $\bar{E}^*$, thus imperfectly implementing the self-consistent approximation.)

Since the present work addresses only small crack density, Hoenig's (1978, 1979) expressions must be linearized in η_c. The dependence of the $\bar{\beta}_j^*$ on η_c is of second order, hence, in the linearization, $\bar{\beta}_j^*$ depends only on the properties of the solid, so the bar and asterisk may be omitted. The linearization yields

$$\beta_2 = \frac{32}{\pi}\left(\frac{1-\nu_s^2}{2-\nu_s}\right) \tag{A12a}$$

and

$$\beta_3 = \frac{4}{\pi}(1-\nu_s^2). \tag{A12b}$$

These are equivalent to previous results (Eshelby 1957) for cracks in an isotropic medium. Hence, using also (3b) and (A2), we have

$$\left\langle \frac{\varepsilon_{13}^c(13)}{2\bar{\sigma}_{23}} \right\rangle^* = \frac{16}{3}\left(\frac{1-\nu_s}{2-\nu_s}\right)\frac{\eta_c}{\mu_s \phi_c} \equiv \frac{B_c(\nu_s)}{\mu_s}\frac{\eta_c}{\phi_c} \tag{A13a}$$

and

$$\left\langle \frac{\varepsilon_{mm}^c(jj)}{-\bar{p}} \right\rangle^* = \frac{16}{9}\left(\frac{1-\nu_s^2}{1-2\nu_s}\right)\frac{\eta_c}{K_s \phi_c} = \frac{A_c(\nu_s)}{K_s}\frac{\eta_c}{\phi_c}, \tag{A13b}$$

implicitly defining coefficients B_c and A_c.

Combining (A2), (A5), (A6), (A10), (A13), (A14), we finally have equations for the moduli affected by cracks,

$$\frac{1}{\mu} = \frac{1}{\mu_s}[1 + B_c(\nu_s)\eta_c] \tag{A14a}$$

and

$$\frac{1}{E} = \frac{1}{E_s}\left[1 + \frac{16}{3}\left(1 - \frac{K_f}{K_s}\right)(1-\nu_s^2)D_c\eta_c\right], \tag{A14b}$$

where D_c is given by (7b) in the main text.

These equations replace (3.6) and (4.11) respectively of Hoenig (1979). They have been linearized in small η_c, and generalized to avoid the neglect of K_f/K_s. They are valid for any fluid saturant; empty cracks correspond to $K_f = 0$. Note that D_c (equation (7b)) contains a non-linear term in the composite parameter $(K_f/K_s)(\eta_c/\phi_c)$; this obviously does not violate the linearization in η_c itself. In fact, D_c must have this form in order to exhibit the correct B–G difference between dry and saturated moduli. In the corresponding quantity D of Budiansky and O'Connell (1976), or O'Connell and Budiansky (1977), the term $-K_f/K_s$ was implicitly neglected, although it follows directly from the exact expressions (A4)–(A9); this omission was corrected by Budiansky and O'Connell (1980). Hoenig (1978) neglected it explicitly. Hudson (1980, 1981) omitted it in his equivalents to both (7b) and (A14b). With the inclusion of these terms, one sees that the limiting case

of stiff fluid (e.g. $K_f = K_s$, as with partially molten aesthenospheric rock) leads to vanishing ε, i.e. to the same result as for vanishing aspect ratio c/a (cf. (8)).

It is now possible to derive equations for the elastic wave velocities. The five parameters (α_0, β_0, δ, ε, γ) required for (1) are given by Thomsen (1986) in terms of the elastic moduli $C_{\alpha\beta}$. Other measures of anisotropy may be defined (cf. e.g. the related set discussed by Lyakhovitskiy (1981)); those used here lead to simplicity in the velocities.

The connections between the $M_{\alpha\beta}$ and the $C_{\alpha\beta}$ are the standard ones for hexagonal symmetry, given by Nye (1957), for example. For the special case of parallel cracks (A1b), the five parameters assume the form

$$\alpha_0 = \alpha_s/[1 + 2((1 - \nu_s)^2/(1 - \nu_s))\varepsilon]^{1/2}, \tag{A15a}$$

$$\beta_0 = \left\{\frac{\bar{\mu}}{\rho}\right\}^{1/2} = \beta_s/\{1 + 2\gamma\}^{1/2}, \tag{A15b}$$

$$\delta = \frac{\Delta}{(1 - \nu_s)(1 - \Delta)}, \tag{A15c}$$

where

$$\Delta = \frac{\bar{\mu}}{\mu_s}\left(\frac{E_s}{\bar{E}} - 1\right)\frac{(1 - \nu_s)}{(1 + \nu_s)} + \left(\frac{\bar{\mu}}{\mu_s} - 1\right)(1 - 2\nu_s), \tag{A15d}$$

$$\varepsilon = \frac{1}{2(1 - \nu_s^2)}\left(\frac{E_s}{\bar{E}} - 1\right), \tag{A15e}$$

$$\gamma = \frac{1}{2}\left(\frac{\mu_s}{\bar{\mu}} - 1\right). \tag{A15f}$$

For the case of weak anisotropy, δ simplifies further to

$$\delta = \left(\frac{E_s}{\bar{E}} - 1\right)\frac{1}{1 + \nu_s} - \left(\frac{\mu_s}{\bar{\mu}} - 1\right)\frac{1 - 2\nu_s}{1 - \nu_s}. \tag{A15g}$$

Using (1) and (A15) at $\theta = 90°$, one may find an expression linking $\bar{v}_p(90°)$ and α_s which has the same form as (4). (These omit the subscripts s on α, β and ν, since they pertain to the case of Arbitrary matrix Appendix § II.)

Independent of this particular model for the cracks, the constraint (A3) may be written, in the case of weak anisotropy, as

$$\delta = 2(1 - v_s)\varepsilon - 2\left(\frac{1 - 2\nu_s}{1 - \nu_s}\right)\gamma = \frac{\varepsilon}{[1 - \beta_0^2/\alpha_0^2]} - 4\frac{\beta_0^2}{\alpha_0^2}\gamma \approx \frac{4}{3}\varepsilon - \gamma, \tag{A16}$$

where the last approximation assumes that $\alpha_0/\beta_0 \approx 2$. Finally, (A15) and (A16) may be combined to express these anisotropy parameters in terms of the crack density, as given by (6) and (7b) in the main text.

Anderson, Minster and Cole (1974) have given numerical calculations based on the work of Eshelby (1957), which appear to be consistent with these results.

II. Arbitrary matrix

The previous case assumed that no porosity was present, except for the aligned cracks. Including the additional effects of arbitrary isotropic porosity and cracks, the elastic compliance matrix $\bar{\mathbf{M}}$ has the same form as in (A1b), but with quantities E, μ, and ν (affected by the presence of the isotropic pore space) replacing the corresponding parameters of the solid. Equation (A4) may be generalized (without further approximation) to

$$\bar{M}_{ijmn}\bar{\sigma}_{mn} = M^{s}_{ijmn}\bar{\sigma}_{mn} + \phi_i\langle\varepsilon^{i}_{ij}\rangle + \phi_c\langle\varepsilon^{c}_{ij}\rangle + (\phi_i p^{i}_{f} + \phi_c p^{c}_{f})M^{s}_{ijkk}. \tag{A17}$$

The second term is the isotropic porosity ϕ_i (consisting of equant porosity, randomly oriented cracks, pore throats, etc.), multiplied by the average strain in this pore space. p^{i}_{f} and p^{c}_{f} are the fluid pressures in the respective parts of the pore space, assumed uniform in each case.

We need to determine particular instances of (A17) which specify the four required moduli E, m, $\bar{E}$, $\bar{\mu}$. The critical step is to establish the compliance differences, independently of the isotropic porosity.

For the shear moduli, using the same logic which led to (A5),

$$\frac{1}{\mu} = \frac{1}{\mu_s} + \phi_i\left\langle\frac{\varepsilon^{i}_{12}(12)}{2\bar{\sigma}_{12}}\right\rangle \tag{A18a}$$

and

$$\frac{1}{\bar{\mu}} = \frac{1}{\mu_s} + \phi_c\left\langle\frac{\varepsilon^{c}_{13}(13)}{2\bar{\sigma}_{13}}\right\rangle + \phi_i\left\langle\frac{\varepsilon^{i}_{13}(13)}{2\bar{\sigma}_{13}}\right\rangle = \frac{1}{\mu} + \phi_c\left\langle\frac{\varepsilon^{c}_{13}(13)}{2\sigma_{13}}\right\rangle. \tag{A18b}$$

For the bulk modulus, using the same logic which led to (A7),

$$\frac{1}{\bar{K}} = \frac{1}{K_s} + \phi_c\left\langle\frac{\varepsilon^{c}_{mm}(jj)}{-\bar{p}}\right\rangle + \phi_i\left\langle\frac{\varepsilon^{i}_{mm}(jj)}{-\bar{p}}\right\rangle - \frac{p^{c}_{f}\phi_c + p^{i}_{f}\phi_i}{\bar{p}K_s}, \tag{A19}$$

of which the isotropic part is

$$\frac{1}{K} \equiv \frac{1}{K_s} + \phi_i\left\langle\frac{\varepsilon^{i}_{mm}(jj)}{-\bar{p}}\right\rangle - \frac{p^{i}_{f}\phi_i}{\bar{p}K_s}. \tag{A20}$$

Addressing the issue of saturation, we must consider the fluid-pressure variation within the pore space. Since different parts of the pore-space have different compliances, we must recognize the possibility of fluid squirt from one portion to another, hence the time available for such squirting, hence the frequency of the excitation.

At sufficiently low frequencies, the fluid pressures in all portions of the pore space have time to equalize, i.e. $p^{i}_{f} = p^{c}_{f} = p_f$. Rewriting (A8) and (A9) to show the different portions of the pore space explicitly,

$$\phi_c\left\langle\frac{\varepsilon^{c}_{mm}(jj)}{-\bar{p}}\right\rangle + \phi_i\left\langle\frac{\varepsilon^{i}_{mm}(jj)}{-\bar{p}}\right\rangle - \frac{p_f\phi}{\bar{p}K_s} = \left[\frac{1}{\bar{K}^{*}} - \frac{1}{K_s}\right]\left(1 - \frac{K_f}{K_s}\right)D_p, \tag{A21}$$

where $\phi = \phi_c + \phi_i$ is the total porosity. In this context,

$$p_f = -K_f\left(\frac{\phi_c}{\phi}\langle e^c_{mm}(jj)\rangle + \frac{\phi_i}{\phi}\langle e^i_{mm}(jj)\rangle\right), \tag{A22}$$

and the derivation proceeds as before. Then, combining (A19) and (A21),

$$\frac{1}{\bar{K}} = \frac{1}{K_s} + \left(1 - \frac{K_f}{K_s}\right)\left[\frac{1}{\bar{K}^*} - \frac{1}{K_s}\right]D_p. \tag{A23}$$

The isotropic part of this is

$$\frac{1}{K} = \frac{1}{K_s} + \left(1 - \frac{K_f}{K_s}\right)\left[\frac{1}{\bar{K}^*} - \frac{1}{K_s}\right]D_p = \frac{1}{K_s} + \left(1 - \frac{K_f}{K_s}\right)\phi_i\left\langle\frac{\varepsilon^i_{mm}(jj)}{-\bar{p}}\right\rangle^* D_p, \tag{A24}$$

so that, using (A19) and (A20),

$$\frac{1}{\bar{K}} = \frac{1}{K} + \left(1 - \frac{K_f}{K_s}\right)\left[\frac{1}{\bar{K}^*} - \frac{1}{K^*}\right]D_p = \frac{1}{K} + \left(1 - \frac{K_f}{K_s}\right)\phi_c\left\langle\frac{\varepsilon^c_{mm}(jj)}{-\bar{p}}\right\rangle^* D_p, \tag{A25}$$

which is similar in form to (A10).

The next task is to define the dry strains $\langle\varepsilon^c_{13}(13)\rangle^*$ and $\langle\varepsilon^c_{mm}(jj)\rangle^*$ in (A18b) and (A25). Since these strains are due to a dilute distribution of aligned cracks, we make the approximation that they are given by the linear expressions (A11) for cracks in a medium with the same Poisson's ratio (ν^*) as the dry, porous, isotropic rock, without aligned cracks:

$$\left\langle\frac{\varepsilon^c_{13}(13)}{2\bar{\sigma}_{13}}\right\rangle^* = \frac{16}{3}\left(\frac{1-\nu^*}{2-\nu^*}\right)\frac{\eta_c}{\mu\phi_c} \equiv \frac{B_c(\nu^*)}{\mu}\frac{\eta_c}{\phi_c} \tag{A26a}$$

and

$$\left\langle\frac{\varepsilon^c_{mm}(ii)}{-\bar{p}}\right\rangle^* = \frac{16}{9}\left(\frac{1-\nu^{*2}}{1-2\nu^*}\right)\frac{\eta_c}{K^*\phi_c} = \frac{A_c(\nu^*)}{K^*}\frac{\eta_c}{\phi_c}. \tag{A26b}$$

This approximation might lead to error if the pores and cracks are of the same size. However, given the modest sensitivity of the coefficients A_c and B_c, within the limited range of their argument ν^*, the approximation is viewed as non-crucial. In any case, the real test of the approximation occurs in its application to real data.

From (A18b), the shear modulus is then

$$\frac{1}{\bar{\mu}} = \frac{1}{\mu}\left[1 + B_c(\nu^*)\eta_c\right], \tag{A27}$$

independent of the fluid content and of the frequency. Combining (A9b) (A25) and (A26b) leads to

$$\frac{1}{\bar{E}} - \frac{1}{E} = \frac{1}{\bar{K}} - \frac{1}{K} = \left(1 - \frac{K_f}{K_s}\right)\frac{A_c(\nu^*)\eta_c}{K^*}D_{ci}(\text{lo}) \quad \ldots \text{low frequency}, \tag{A28}$$

where $D_{ci}(\mathrm{lo})$ is given by (5a) in the main text. Equations (A27) and (A28) define the compliance differences needed to specify the anisotropies, given by equations of the same form as (A15), but without the subscripts s. The results are shown explicitly in (2) in the main text.

Alternatively, at the 'moderately high' frequencies defined in the main text, the cracks are hydraulically unconnected with the isotropic pore space, so that this isotropic pore space acts like the solid in (A9). Replacing K_s with K in (7) and (A10), we have

$$\frac{1}{\bar{E}} - \frac{1}{E} = \frac{1}{\bar{K}} - \frac{1}{K} = \left(1 - \frac{K_f}{K_s}\right) \frac{A_c(\nu^*)\eta_c}{K} D_{ci}(\mathrm{mh}) \quad \ldots \text{'moderately high' frequency,} \tag{A29}$$

where $D_{ci}(\mathrm{mh})$ is given by (5b) in the main text. Equations (A27) and (A29) define the compliance differences needed to specify the velocities and anisotropies at 'moderately high' frequencies, given by equations of the same form as (A15), but without the subscripts s. The results are shown explicitly in (2).

III. Modelled matrix

In a case where the isotopic, porous matrix may itself be modelled as a dilute distribution of spherical pores in an isotropic solid, the shear stress-strain ratio in (A18a) is given by (Budiansky and O'Connell 1980)

$$\left\langle \frac{\varepsilon^i_{12}(12)}{2\bar{\sigma}_{12}} \right\rangle^* = \frac{15(1-\nu_s)}{(7-5\nu_s)\mu_s} \equiv \frac{B_p(\nu_s)}{\mu_s}, \tag{A30a}$$

defining coefficient B_p as analogous to B_c, (A13a). Similarly, the bulk stress-strain ratio in the pores is given by (Budiansky and O'Connell 1980)

$$\left\langle \frac{\varepsilon^i_{mm}(jj)}{-\bar{p}} \right\rangle^* = \frac{3}{2} \frac{(1-\nu_s)}{(1-2\nu_s)K_s} \equiv \frac{A_p(\nu_s)}{K_s}, \tag{A30b}$$

defining coefficient A_p as analogous to A_c, (A13b). Then, combining (A9b), (A13b), (A19) and (A30b) leads to the fluid influence factor in (7a), which is very similar to that derived by Budiansky and O'Connell (1980).

References

Aki K. and Richards P.G. 1980. Quantitative Seismology: Theory and Methods. *W.H. Freeman, San Francisco.*

Anderson D.L., Minster B. and Cole D. 1974. The effect of oriented cracks on seismic velocities. *Journal of Geophysical Research* 79, 4011–4016.

Biot M.A. 1941. General theory of three-dimensional consolidation. *Journal of Applied Physics* 12, 155–164.

Budiansky B. and O'Connell R.J. 1976. Elastic moduli of a cracked solid. *International Journal of Solids and Structures* 12, 81–97.

Budiansky B, and O'Connell R.J. 1980. Bulk dissipation in heterogeneous media. *Solid Earth Geophysics and Geotechnic* **ASME-AMD 42**, 1–10.

Crampin S. 1978. Seismic-wave propagation through a cracked solid: polarization as a possible dilatancy diagnostic. *Geophysical Journal of the Royal Astronomical Society* 53, 467–496.

Crampin S. 1981. A review of wave motion in anisotropic and cracked elastic media. *Wave Motion* 3, 343–391.

Crampin S. 1984. Effective anisotropic elastic constants for wave propagation through cracked solids. *Geophysical Journal of the Royal Astronomical Society* 76, 135–145.

Crampin S. 1985. Evaluation of Anisotropy by shear-wave splitting. *Geophysics* 50, 343–391.

Crampin S., McGonigle R. and Masataka A. 1986. Extensive-dilatancy anisotropy beneath Mt. Hood, Oregon, and the effect of aspect ratio of seismic velocities through aligned cracks. *Journal of Geophysical Research* 91, 12703–12710.

Eshelby J.D. 1957. The determination of the elastic field of an ellipsoidal inclusion, and related problems. *Proceedings of the Royal Society* A241, 376–396.

Garbin H.D. and Knopoff L. 1973. The compressional modulus of a material permeated by a random distribution of circular cracks. *Quarterly of Applied Mathematics* 30, 453–464.

Garbin H.D. and Knopoff L. 1975a. The shear modulus of a material permeated by a random distribution of free circular cracks. *Quarterly of Applied Mathematics* 33, 296–300.

Garbin H.D. and Knopoff L. 1975b. Elastic moduli of a medium with liquid-filled cracks. *Quarterly of Applied Mathematics* 33, 301–303.

Gassmann F. 1951. Über die Elastizität poroser Medien. *Mitteilungen aus dem inst. für Geophysik* (Zürich) 17, 1–23.

Hill R. 1963. Elastic properties of reinforced solids: some theoretical principles. *Journal of the Mechanics and Physics of Solids* 11, 357–372.

Hoenig A. 1978. The behavior of a flat elliptical crack in an anisotropic elastic body. *International Journal of Solids and Structures* 14, 925–934.

Hoenig A. 1979. Elastic moduli of the non-randomly cracked body. *International Journal of Solids and Structures* 15, 137–154.

Hudson J.A. 1980. Overall properties of a cracked solid. *Mathematical Proceedings of the Cambridge Philosophical Society* 88, 371–384.

Hudson J.A. 1981. Wave speeds and attenuation of elastic waves in material containing cracks. *Geophysical Journal of the Royal Astronomical Society* 64, 133–150.

Lyakhovitskiy F.M. 1981. Discussion: On Berryman and Levin. *Geophysics* 46, 336–339.

Mavko G. and Jizba D. 1991. Estimating grain-scale effects on velocity dispersion in rocks. *Geophysics* 56, 1940–1949.

Nye J.F. 1957. Physical Properties of Crystals. *Oxford Press, New York.*

O'Connell R.J. and Budiansky B. 1974. Seismic velocities in dry and saturated cracked solids. *Journal of Geophysical Research* 79, 5412–5426.

O'Connell R.J. and Budiansky B. 1977. Viscoelastic properties of fluid-saturated cracked solids. *Journal of Geophysical Research* 82, 5719–5736.

Rathore J.S., Fjaer E., Holt R.M. and Renlie L. 1991. Acoustic anisotropy in synthetics with controlled crack geometry. 53rd EAEG meeting, Florence, Italy, Expanded Abstracts, 167–168.

Rathore J.S. Fjaer E., Holt R.M. and Renlie L. 1995. Acoustic anisotropy of a synthetic sandstone with controlled crack geometry. *Geophysical Prospecting*, this issue.

Schoenberg M. and Muir F. 1989. A calculus for finely layered anisotropic media. *Geophysics* 54, 581–589.

Shearer P. and Orcutt J. 1985. Anisotropy in the oceanic lithosphere-theory and observations from the Negendei seismic refraction experiment in the south-west Pacific. *Geophysical Journal of the Royal Astronomical Society* 80, 493–526.

Shearer P.M. Orcutt J. 1986. Compressional and shear wave anisotropy in the oceanic lithosphere-the Negendei seismic refraction experiment. *Geophysical Journal of the Royal Astronomical Society* 87, 967–1003.

Stephen R.A. 1985. Seismic anisotropy in the upper oceanic crust. *Journal of Geophysical Research* 90, 11 383–11 396.

Thomsen L. 1985. Biot-consistent elastic moduli of porous rocks: low-frequency limit. *Geophysics* 50, 2797–2708.

Thomsen L. 1986. Weak elastic anisotropy. *Geophysics* 51, 1954–1966.

Walsh J.B. 1969. New analysis of attenuation in partially melted rock. *Journal of Geophysical Research* 17, 4333–4337.

Watt J.P., Davies G.F. and O' Connell R. 1976. The elastic properties of composite material. *Reviews of Geophysics and Space Physics* 14, 541–563.

White R.S. and Whitmarsh R.B. 1984. An investigation of seismic anisotropy due to cracks in the upper oceanic crust at 45° N, mid-Atlantic ridge. *Geophysical Journal of the Royal Astronomical Society* 71, 439–467.

(1978, 1979); we consider first the case of cracks only. The elastic compliance tensor M_{ijkl} of a transversely isotropic body may be written as a two-dimensional symmetric matrix $M_{\alpha\beta}$ following the usual Voigt recipe:

$$\mathbf{M} = \begin{bmatrix} \frac{1}{E_{11}} & \left(\frac{1}{E_{11}} - \frac{1}{2\mu_{66}}\right) & -\frac{1}{E_{13}} & & & \\ & \frac{1}{E_{11}} & -\frac{1}{E_{13}} & & & \\ & & \frac{1}{E_{33}} & & & \\ & & & \frac{1}{\mu_{44}} & & \\ & & & & \frac{1}{\mu_{44}} & \\ & & & & & \frac{1}{\mu_{66}} \end{bmatrix}. \tag{A1a}$$

Only the non-zero elements of the upper triangle are shown. There are five independent elastic compliances.

If the anisotropy is caused by parallel cracks lying in the 3-plane of an isotropic solid, then the only strain components affected by the cracks have subscripts 13, 23 and 33 (the last only when the stress is also 33). In this case, (A1a) reduces to the special form

$$\bar{\mathbf{M}} = \begin{bmatrix} 1/E_s & -\nu_s/E_s & -\nu_s/E_s & & & \\ & 1/E_s & -\nu_s/E_s & & & \\ & & 1/\bar{E} & & & \\ & & & 1/\bar{\mu} & & \\ & & & & 1/\bar{\mu} & \\ & & & & & 1/\mu_s \end{bmatrix}, \tag{A1b}$$

which has only four independent elastic compliances, two of which are shown as the elastic moduli E_s and μ_s of the uncracked solid. Its Poisson's ratio ν_s has the usual connections with the isotropic solid moduli:

$$\nu_s \equiv \frac{E_s}{2\mu_s} - 1 = \frac{1}{2} - \frac{E_s}{6K_s}. \tag{A2}$$

The reduction in degrees of the freedom (from 5 to 4) represented by (A1b) results in a constraint among the five elastic moduli, independent of any particular model for the cracks, so long as they are thin and parallel. This constraint may be written